

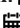
High Pressure Thermoelastic Behaviour of Intermetallic Compound MgCu at Elevated Temperatures

ISSN: 2576-8840



***Corresponding author:** Anand K, Department of Physics, Institute of Basic Sciences, Dr. Bhimrao Aamedkar University, India

Submission:  March 06, 2023

Published:  April 03, 2023

Volume 18 - Issue 4

How to cite this article: Anand K*, Sharma BS, Rajesh K and Singh KS. High Pressure Thermoelastic Behaviour of Intermetallic Compound MgCu at Elevated Temperatures. Res Dev Material Sci. 18(4). RDMS. 000941. 2023.

DOI: [10.31031/RDMS.2023.18.000941](https://doi.org/10.31031/RDMS.2023.18.000941)

Copyright@ Anand K, This article is distributed under the terms of the Creative Commons Attribution 4.0 International License, which permits unrestricted use and redistribution provided that the original author and source are credited.

Anand K^{1*}, Sharma BS¹, Rajesh K² and Singh KS²

¹Department of Physics, Institute of Basic Sciences, Dr. Bhimrao Aamedkar University, India

²Department of Physics, R.B.S. College, India

Abstract

A simple analytical method has been developed using the Grover-Saxena equation of state to determine pressure-volume-temperature relationships, bulk modulus and its pressure derivative, Debye temperature, Grüneisen parameter and melting curve of the intermetallic compound MgCu. We have considered a wide range of pressures up to 50GPa, and temperatures up to 1000K. The effect of temperature has been taken into account in terms of the thermal pressure estimated from the Anderson formula. The results are compared with those obtained by earlier workers using the ab initio calculations based on the density functional theory. The Roy-Sarkar model recently developed for the density dependence of Debye frequency based on the first-principles has been used in the present study to investigate variations of Debye temperature and Grüneisen parameter with pressure and temperature. Melting curve for MgCu has been predicted using the Roy-Sarkar model for the density dependence of gamma in the Lindemann law. The simple analytical methods used in the present study are capable of making rapid estimations of the thermoelastic properties and melting curve for MgCu.

Keywords: Equation of state; Bulk modulus; Debye temperature; Grüneisen parameter; Melting curve; MgCu

Introduction

Intermetallic compounds in general, and Mg based alloys in particular have important applications in various fields of science and technology [1-3]. MgCu with a CsCl (B2) type structure is of current interest [4-6]. Mg-alloys are among the lightest structural materials known, exhibiting remarkable fundamental properties [7-10]. Thermoelastic properties of intermetallic compounds at high pressures and high temperatures have been investigated [11-13] using phenomenological models and ab initio calculations.

The structural and elastic properties of the intermetallic compound MgCu with CsCl-type structure have been investigated [5] using the first-principles DFT calculations [14,15]. It has been emphasized by Daoud et al. [12] that the study performed by Boucetta [5] was established only at zero pressure for the thermodynamic properties of MgCu up to a temperature of 1000K. The effect of high pressure on the thermodynamic properties of MgCu with CsCl (B2) structure has been investigated [12] using the plane-wave pseudopotential (PW-PP) method [16] within the framework of DFT.

In the present study, we use a simple analytical method based on the Grover-Saxena equation of state (EOS) [17,18]. This EOS [19] has been found to yield good agreement with the available experimental data [20-26] and ab initio results [27,28] for different types of compounds. In the present work, we use this EOS for investigating thermodynamic and thermoelastic behaviour of MgCu up to a pressure of 50GPa and temperatures up to 1000K. The model for density dependence of the Debye frequency developed by Roy [29] based on the DFT calculations [30,31] for some elemental solids, when used in the Lindemann law of melting [32,33], gives good agreement with the available experimental data [34-38]. Subsequently, Anand et al. [39] have demonstrated the adequacy of the Roy-Sarkar model also for determining melting curves of various diatomic compounds in good agreement with the available experimental data [40-42] as well as with the results based on the ab initio molecular dynamics [42-45] and the DFT-LDA method [46]. In the present study, we use

the Roy-Sarkar model in the Lindemann law to determine melting curve of the intermetallic compound MgCu.

Method of Analysis

Volume of a material at high pressures and high temperatures can be determined with the help of the Grover-Saxena EOS that can be written as follows [19]

$$\frac{V(T,P)}{V(300,0)} = 1 - \frac{1}{(K'_0 + 1)} \ln \left[1 + \frac{(K'_0 + 1)}{K_0} (P - \Delta P_{th}) \right] \quad (1)$$

Where P is the total pressure. K_0 and K'_0 are respectively the bulk modulus and its pressure derivative, both at zero-pressure and at temperature equal to 300K. ΔP_{th} is the difference

$$\Delta P_{th} = P_{th}(T) - P_{th}(300) \quad (2)$$

Where $P_{th}(T)$ and $P_{th}(300)$ are the values of thermal pressure at temperatures T and 300K, respectively. It has been found by Anderson [47] that the thermal pressure changes linearly with temperature at high temperatures, and we can write [48,49]

$$\Delta P_{th} = \alpha K_T (T - T_0) \quad (3)$$

Where α is the thermal expansivity and K_T the isothermal bulk modulus, both at the initial temperature $T_0 = 300$ K. At temperatures $T \geq \theta_D$, the Debye temperature, the product αK_T remains nearly constant [47]. We have taken $\alpha = 8.35 \times 10^{-5} K^{-1}$, and $K_T = 59.58$ GPa for MgCu at ambient conditions [12].

Expressions for bulk modulus $K(T,P)$ and its pressure derivative $K'(T,P)$ are obtained by differentiating Eq. (1) successively with respect to pressure. Thus, we get

$$\frac{K(T,P)}{K(300,0)} = \frac{V(T,P)}{V(300,0)} \left[1 + \frac{(K'_0 + 1)}{K_0} (P - \Delta P_{th}) \right] \quad (4)$$

And

$$K'(T,P) = (K'_0 + 1) \frac{V(T,P)}{V(300,0)} - 1 \quad (5)$$

Where $K_0 = 59.58$ GPa, and $K'_0 = 4.05$ for MgCu [12]. Equations (1), (4) and (5) are used to calculate $V(T,P)$, $K(T,P)$ and $K'(T,P)$ for MgCu at high pressures and high temperatures. The results are given in Figures 1-3.

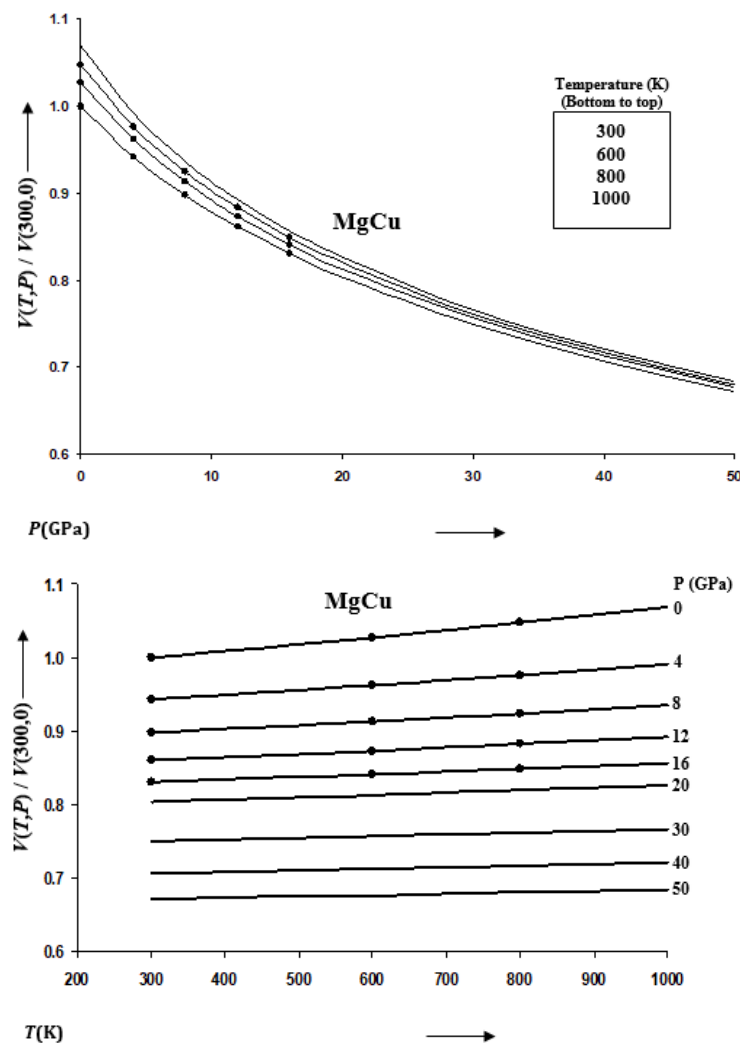


Figure 1: Variations of $V(T,P)/V(300,0)$ with pressure along selected isotherms, and with temperature along selected isobars for MgCu shown by continuous curves (—). Symbols (●) represent the first-principles DFT calculations [12].

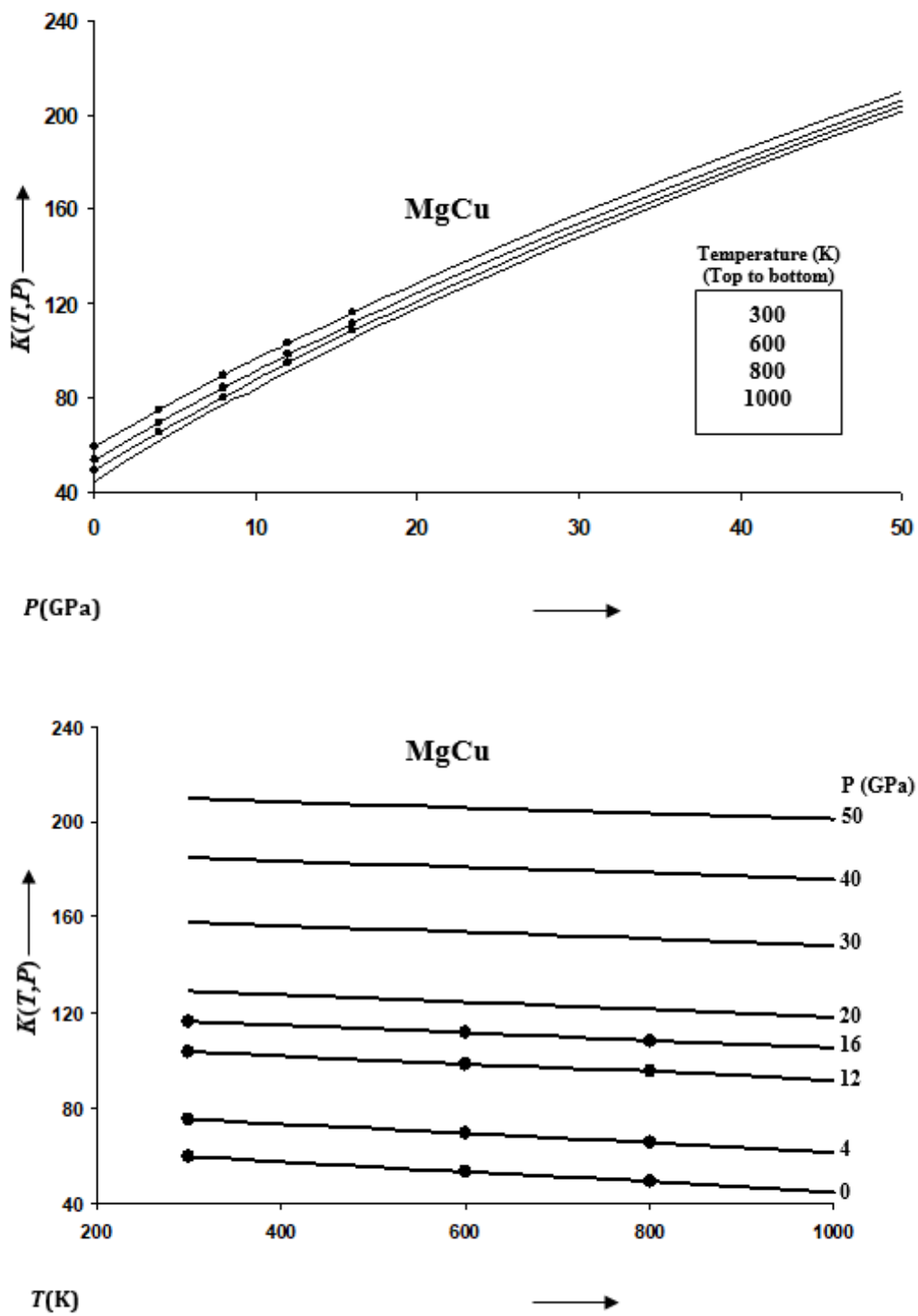


Figure 2: Variations of $K(T,P)$ with pressure along selected isotherms, and with temperature along selected isobars for MgCu shown by continuous curves (—). Symbols (●) represent the first-principles DFT calculations [12].

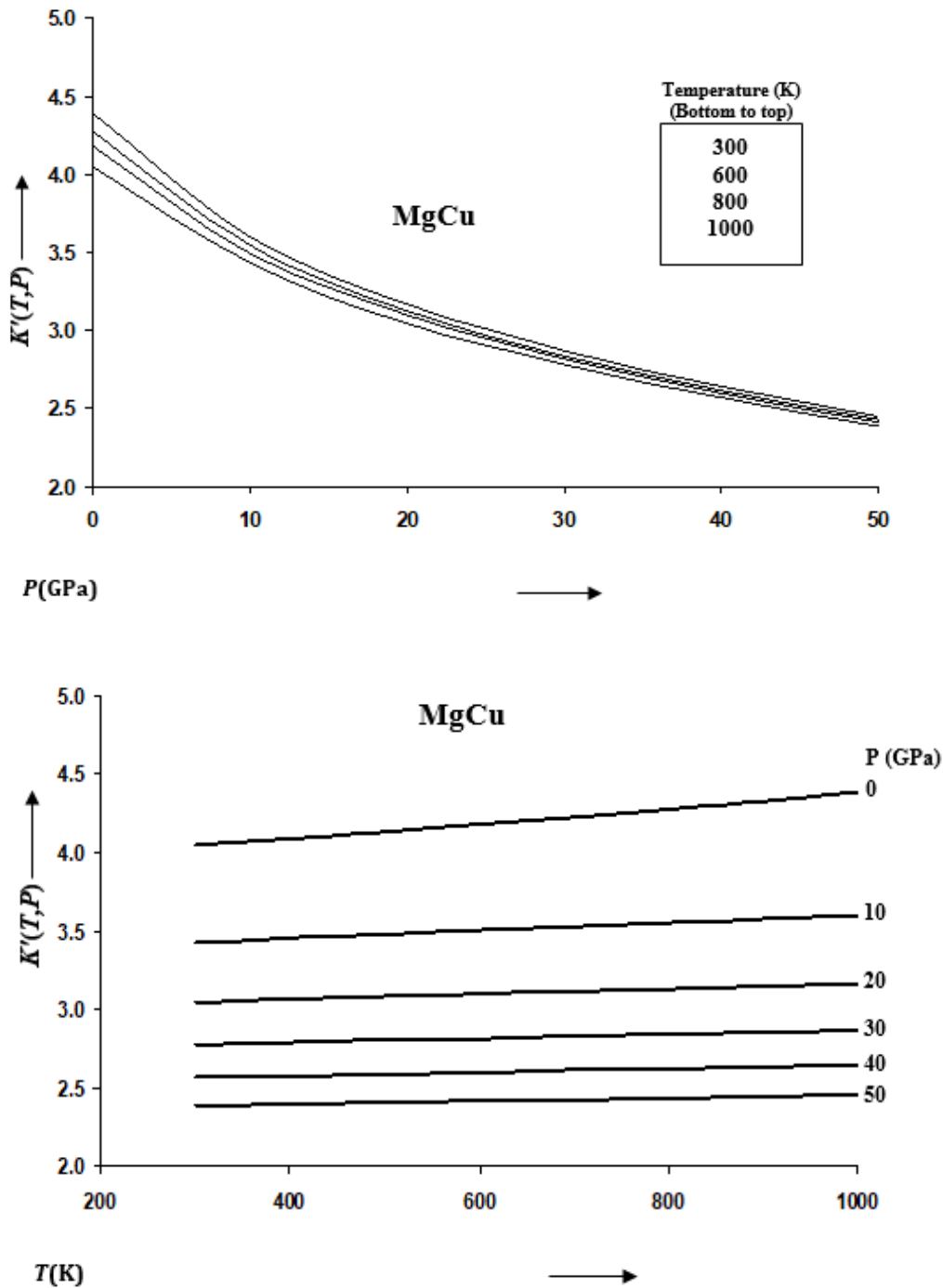


Figure 3: Variations of $K'(T,P)$ with pressure along selected isotherms, and with temperature along selected isobars for MgCu shown by continuous curves (—).

The Grüneisen parameter γ can be expressed as a function of volume ratio V/V_0 as follows [39]

$$\gamma = \frac{\gamma_0}{\gamma_0 - (\gamma_0 - 1)V/V_0} \quad (6)$$

Eq. (6) has been obtained [39] by using the linear dependence formulations for the Debye frequency [29]. In Eq.

(6), $\gamma_0 = \gamma(300, 0) = 2.08$, and $V_0 = V(300, 0)$. Values of γ for MgCu at different pressures and temperatures are shown in Figure 4. For determining the Debye temperature θ_D we use the following relationship for gamma

$$\gamma = -\frac{d \ln \theta_D}{d \ln V} \quad (7)$$

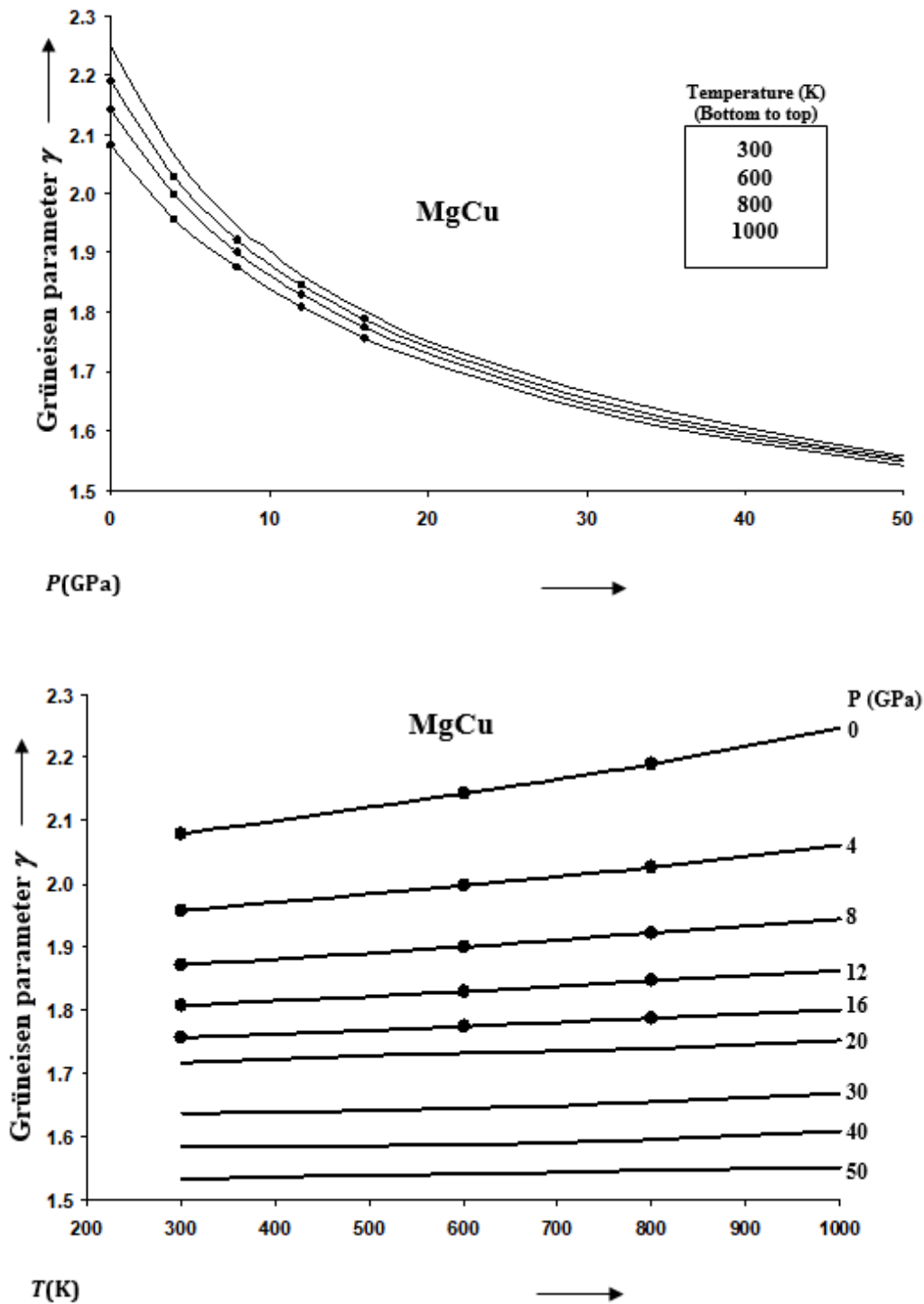


Figure 4: Variations of Grüneisen parameter γ with pressure along selected isotherms, and with temperature along selected isobars for MgCu shown by continuous curves (—). Symbols (●) represent the first-principles DFT calculations [12].

Taking Eqs. (6) and (7) together, and then integrating we find

$$\theta_D(T, P) = \theta_D(300, 0) \left[\frac{\gamma_0 V(300, 0)}{V(T, P)} - (\gamma_0 - 1) \right] \quad (8)$$

Eq. (8) has been obtained and reported for the first time in the present study. Variations of θ_D with P and T for MgCu are given in Figure 5. Value of $\theta_D(300, 0)$ is equal to 373.5K for MgCu [12].

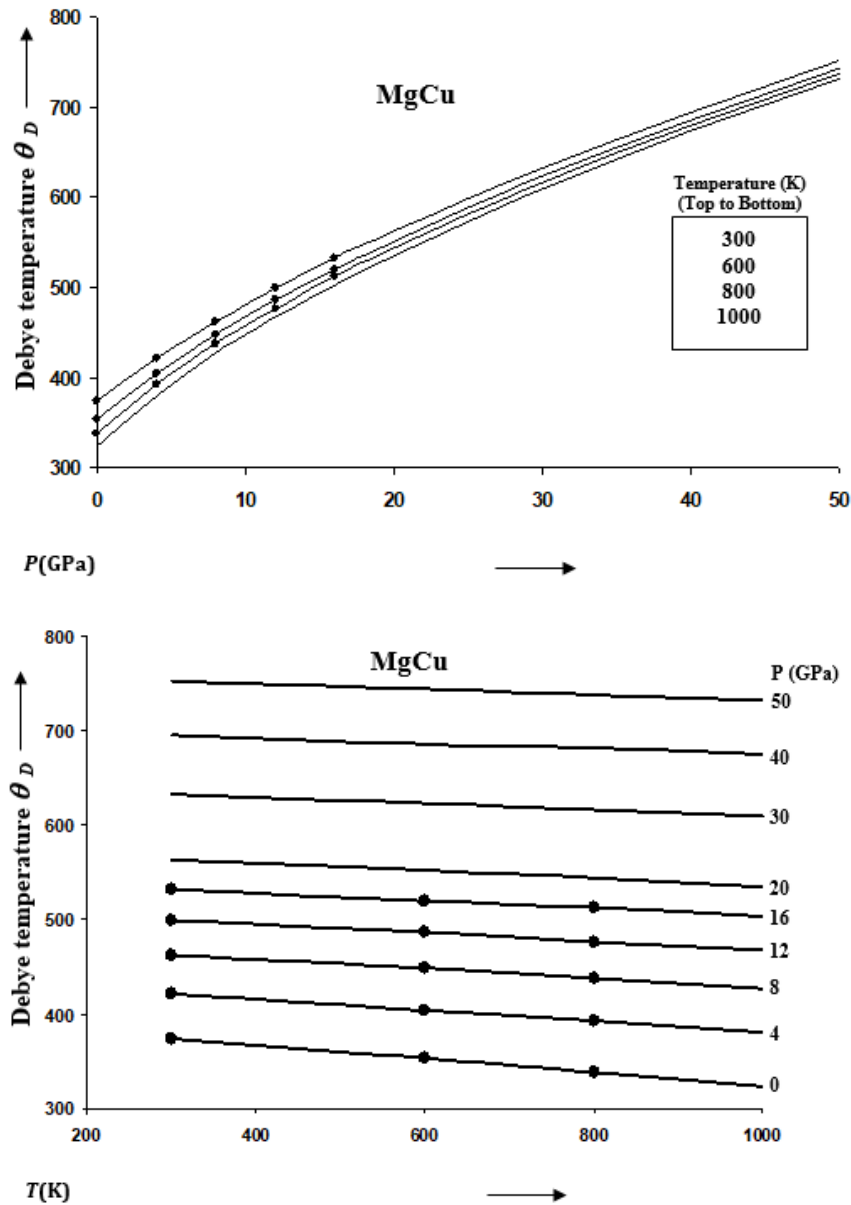


Figure 5: Variations of Debye temperature θ_D with pressure along selected isotherms, and with temperature along selected isobars for MgCu shown by continuous curves (—). Symbols (•) represent the first-principles DFT calculations [12].

Equation (6) for the volume dependence of gamma when used in the Lindemann law of melting [32,33] gives the following expression [29,39]

$$\frac{T_m}{T_{m0}} = \left(\frac{V}{V_0}\right)^{-4/3} \left[\gamma_0 - (\gamma_0 - 1) \frac{V}{V_0} \right]^2 \quad (9)$$

Where T_{m0} is the value of melting temperature T_m at zero-pressure. Values of T_{m0} are available for MgCu_2 and Mg_2Cu [50] which are respectively 1093K and 990K. For the intermetallic compound MgCu, we take an intermediate value for T_{m0} equal to 1042K. Melting curve for MgCu is determined from Eq. (9) by calculating melting temperatures at high pressures. An expression for the melting slope at ambient pressure ($P=0$) is given below [39]

$$\left(\frac{dT_m}{dP}\right)_{P=0} = 2 \left(\gamma_0 - \frac{1}{3} \right) \frac{T_{m0}}{K_0} \quad (10)$$

Equation (10) gives dT_m/dP at ambient pressure equal to 61KPa^{-1} for MgCu. Melting slope of a material decreases with the increase in pressure because gamma decreases and bulk modulus increases with the increasing pressure [51].

Results and Discussion

Results for P-V relationship along different isotherms at selected temperatures obtained from the Grover-Saxena EOS for MgCu are shown in Figure 1. Isobaric variations of volume with temperature at selected pressures for MgCu are also shown in Figure 1. It is found that different isotherms appear to converge at high pressures.

The rate of variation of volume with temperature becomes small at high pressures. This is consistent with the thermodynamics of solids at extreme compression [52,53]. The isothermal and isobaric variations of bulk modulus $K(T,P)$ are given in Figure 2 and those for pressure derivative of bulk modulus $K'(T,P)$ in Figure 3 for MgCu. It is found that K increases and K' decreases with the increase in pressure along an isotherm.

Variations of the Grüneisen parameter γ along different isotherms and isobars obtained from Eq. (6) are shown in Figure 4. It should be mentioned that Eq. (6) satisfies the thermodynamic constraints [39] for the volume derivatives of gamma in the limit of infinite pressure [54,55]. It is found that γ for MgCu decreases substantially with the increase in pressure along an isotherm, and increases slowly with the increase in temperature along an isobar. At high pressures, the variation of gamma with temperature

becomes negligibly small such that γ becomes almost independent of temperature. Another physical quantity of great importance is the Debye temperature for describing the thermodynamic and thermoelastic behaviour of materials at high pressures and high temperatures. We have determined variations of θ_D with pressure as well as with temperature using Eq. (8) and the P-V-T results based on the Grover-Saxena EOS given in Figure 1. The results for the variations of $\theta_D(T,P)$ are shown in Figure 5. The results obtained in the present study are found to compare well (Figures 1, 2, 4 & 5) with the corresponding values determined by Daoud et al. [12] using the first-principles DFT calculations for MgCu. The best fit for the data on $\theta_D(T,P)$ for MgCu [12] can be expressed as a quadratic function of temperature along an isobar

$$\theta_D(T,P) = A - BT - CT^2 \quad (11)$$

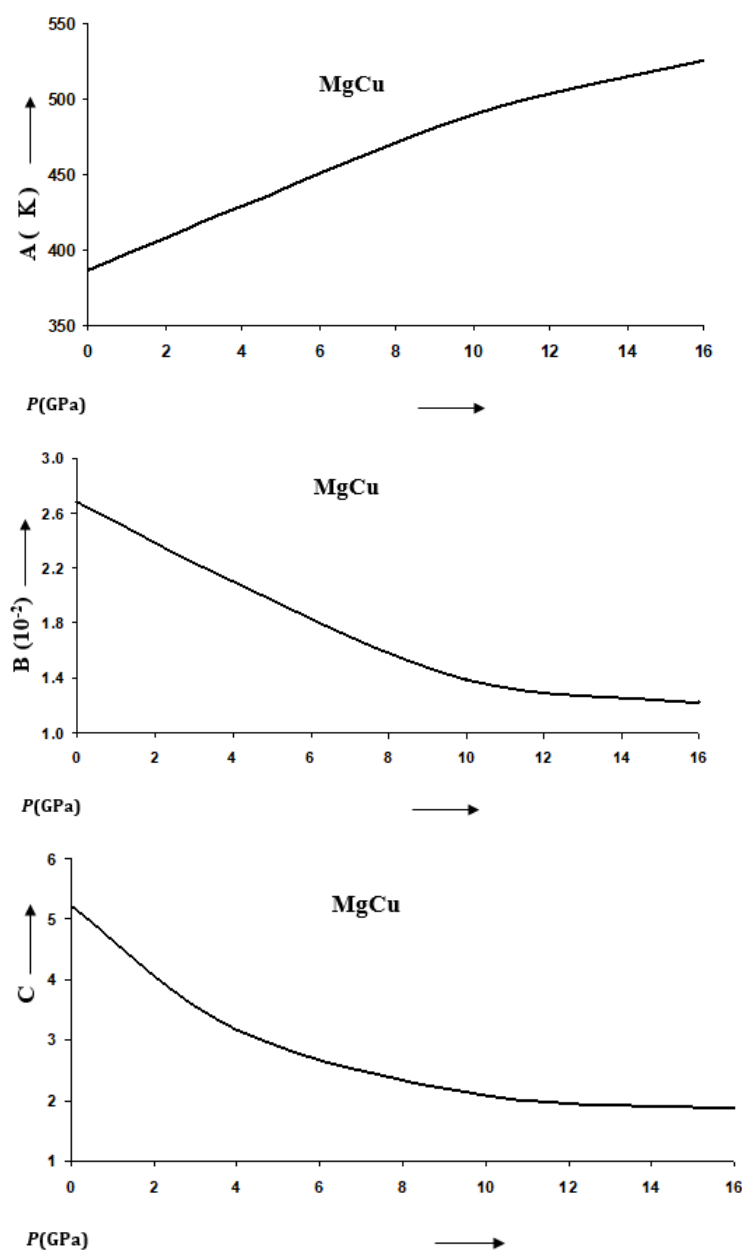


Figure 6: Variations of parameters A, B and C appearing in Eq. (11) for the Debye temperature $\theta_D(T,P)$ formulated by Daoud *et al.* [12].

Where A, B and C are constants for a given material at constant pressure. Values of A, B and C change with the variation in pressure as shown in Figure 6 for MgCu based on the results reported by Daoud et al. [12]. Values of A increase with the increase in pressure whereas B and C decrease with P. Thus the effect of temperature is suppressed at high pressures. The rate of decreasing θ_D with temperature becomes small at high pressures. It should be mentioned that θ_D increases with the increase in pressure along an isotherm. The relationship between melting temperature and θ_D has been used in the Lindemann law [32,33] to find that T_m also increases with P. We have calculated values of T_m at different pressures for MgCu using Eq. (9), the Lindemann law based on the

Roy-Sarkar model for the density dependence of Debye frequency [29]. The melting curve for MgCu thus determined is given in Figure 7. It is worth-mentioning here that the ab initio methods based on the DFT calculations and molecular dynamics simulations are very expensive and time-consuming involving heavy computations. Such attempts have also been made in case of MgCu [12] to find the results up to a pressure of 16GPa and temperatures up to 1000K. It is found that the results obtained in the present study using simple analytical methods are in extremely good agreement with the first-principles DFT calculations (Figures 1, 2, 4 & 5).

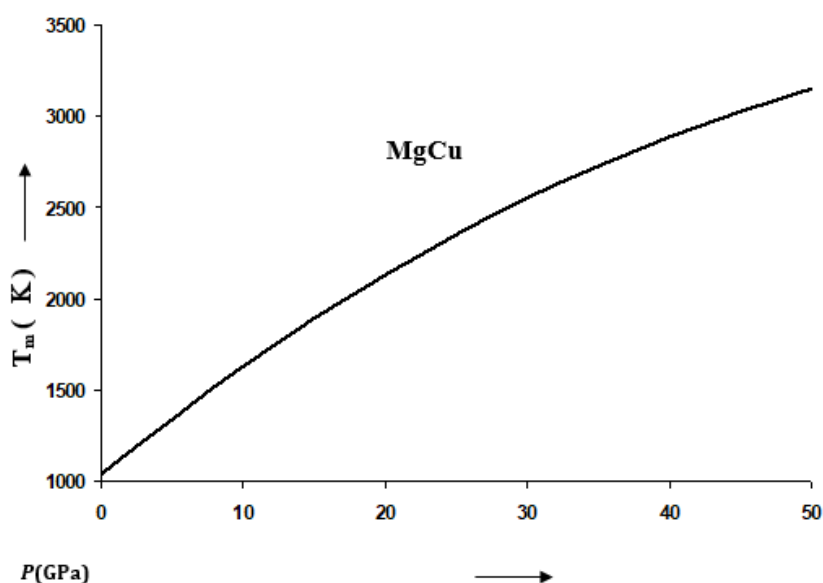


Figure 7: Melting curve of MgCu representing the variations of melting temperature T_m (K) at different pressures calculated from the Lindemann law (Eq. 9) based on the Roy-Sarkar model [29].

Conclusion

A simple method has been developed in the present study using the Grover-Saxena EOS for investigating the thermoelastic properties of MgCu intermetallic compound with CsCl (B2) structure up to a pressure of 50GPa. The effect of temperature up to 1000K has been taken into account in terms of thermal pressure. Pressure-volume-temperature relationships have been predicted along different isotherms at selected temperatures, and along different isobars at selected pressures. Variations of bulk modulus and its pressure derivative with the increase in pressure and temperature have also been determined.

The Roy-Sarkar model based on DFT calculations has been used to determine variations of the Grüneisen parameter and Debye temperature of MgCu with the changes in pressure and temperature. At high pressures, gamma and Debye temperature both become virtually constant, i.e. independent of temperature. The results obtained in the present study for thermoelastic properties of MgCu using simple analytical methods are very close to the first principles DFT calculations reported by Daoud et al. [12]. Using the results for volume dependence of Grüneisen parameter in the Lindemann

law we have determined melting curve for MgCu up to a pressure of 50GPa. The methods used in the present study are capable of making rapid and accurate estimations of the thermoelastic properties and melting curve for MgCu.

References

1. Bioud N, Kassali K, Bouarissa N (2017) Thermodynamic properties of compressed CuX (X = Cl, Br) compounds: Ab initio study. *J Electron Matter* 46(2017): 2521.
2. Bioud N, Sun XW, Daoud S, Song T, Liu ZJ (2018) Structural stability and thermodynamic properties of BSb under high pressure and temperature. *Mater Res Express* 5: 085904.
3. Taylor RH, Curtarolo S, Hart GLW (2011) Guiding the experimental discovery of magnesium alloys. *Phys Rev B* 84: 084101.
4. Watanabe H, Gota Y, Kamegawa A, Takamura H, Okada M (2004) High pressure synthesis of novel compounds in Mg-TM systems (TM = Ti~Zn). *Mater Trans* 45(4): 1350-1354.
5. Boucetta S, Zegrar F (2013) Density functional study of elastic, mechanical and thermodynamic properties of MgCu with a CsCl-type structure. *Magnes J Alloys* 1(2): 128-133.
6. Westbrook JH, Fleischer RL (1995) *Intermetallic compounds-principles and practices*, Wiley, New York, USA.

7. Takamura H, Kakuta H, Goto H, Watanabe H, Kamegawa A, et al. (2005) High-pressure synthesis and energetics of MgCu with a CsCl-type structure. *J Alloys Compd* 404-406: 372-376.
8. Chou HS, Huang JC, Lai YH, Chang LW, Du XH, et al. (2009) Amorphous and nanocrystalline sputtered Mg-Cu thin films. *J Alloys Compd* 483(1-2): 341-345.
9. Ma Z, Liu Y, Yu L, Cai Q (2012) Investigation of phase composition and nanoscale microstructure of high-energy ball-milled MgCu sample. *Nanoscale Res Lett* 7(1): 390.
10. Mezbahul-Islam M, Kevorkov D, Medraj M (2008) The equilibrium phase diagram of the magnesium-copper-yttrium system. *J Chem Thermodynamics* 40(7): 1064-1076.
11. Jha PK (2005) Phonon spectra and vibrational mode instability of MgC Ni₃. *Phys Rev* 72(21): 214502.
12. Daoud S, Bioud N, Saini PK, Magnes J (2019) Finite temperature thermophysical properties of MgCu intermetallic compound from quasi-harmonic Debye model. *Journal of Magnesium and Alloys* 7(2): 335-344.
13. Rajesh K, Singh KS, Anand K (2022) Equation of state, thermoelastic properties and melting curves of some intermetallic compounds LiBC, MgB₂ and TiB₂. *Comp Cond Matter* 32: e00710.
14. Hohenberg P, Kohn W (1964) Inhomogeneous electron gas. *Phys Rev* 136(3B): 864.
15. Kohn W, Sham LJ (1965) Self-consistent equations including exchange and correlation effects. *Phys Rev* 140(4A): 1133.
16. Fuchs M, Scheffler M (1999) Ab initio pseudopotentials for electronic structure calculations of poly-atomic systems using density-functional theory. *Comput Phys Commun* 119(1): 67-98.
17. Grover R, Getting IC, Kennedy GC (1973) Simple compressibility relation for solids. *Phys Rev* 7(2): 567.
18. Saxena SK, Eriksson G (2015) Thermodynamics of iron at extreme pressures and temperatures. *J Phys Chem Solids* 84: 70-74.
19. Anand K, Singh MP, Sharma BS (2019) Analysis of V-P-T relationships and bulk modulus for some geophysically-relevant solids using the Grover-Saxena equation of state. *J Phys Chem Solids* 134: 121-126.
20. Boehler R, Kennedy GC (1980) Equation of state of sodium chloride up to 32 kbar and 500 °C †. *J Phys Chem Solids* 41(5): 517-523.
21. Mao HK, Hemley RJ, Fei Y, Shu JF, Chen IC, et al. (1991) Effect of pressure, temperature, and composition on lattice parameters and density of (Fe, Mg)SiO₃-perovskites to 30GPa. *Journal of Geophysical Research* 96(B5): 8069-8079.
22. Wang YB, Weidner DJ, Guyot F (1996) Thermal equation of state of CaSiO₃ perovskite. *Journal of Geophysical Research* 101(B1): 661-672.
23. Funamori N, Yagi T, Utsuni W, Kondo T, Uchida T, et al. (1996) Thermoelastic properties of MgSiO₃ perovskite determined by in situ X ray observations up to 30 GPa and 2000K. *Journal of Geophysical Research* 101(B4): 8257-8269.
24. Fiquet G, Dewaele A, Andrault D, Kunz M, Levinan T (2000) Thermoelastic properties and crystal structure of MgSiO₃ perovskite at lower mantle pressure and temperature conditions. *Geophys Res Lett* 27(1): 21-24.
25. Guignot N, Andrault D, Morard G, Bolfman-Casanova N, Mezouar M (2007) Thermoelastic properties of post-perovskite phase MgSiO₃ determined experimentally at core-mantle boundary P-T conditions. *Earth Planet Sci Lett* 256(1-2): 162-168.
26. Matsui M, Ito E, Yamazaki D, Yoshino T, Guo X, et al. (2012) Static compression of (Mg_{0.83}, Fe_{0.17})O and (Mg_{0.75}, Fe_{0.25})O ferro periclaise up to 58GPa at 300, 700, and 1100K. *Am Mineral* 97(1): 176.
27. Li L, Donald Weidner J, Brodholt J, Alfe D, Price GD, et al. (2006) Elasticity of CaSiO₃ perovskite at high pressure and high temperature. *Phys Earth Planet Inter* 155(3-4): 249-259.
28. Belmonte D (2017) First principles thermodynamics of minerals at HP-HT conditions: MgO as a prototypical material. *Minerals* 7(10): 183.
29. Roy UC, Sarkar SK (2021) Ab initio study of the density dependence of the Grüneisen parameter at pressures up to 360GPa. *Comp Cond Matter* 27: e00552.
30. Martin RM (2001) *Electronic structure: Basic theory and practical methods*. (2nd edn), Cambridge University Press, UK.
31. Baroni S, Gironcoli SD, Corso AD, Giannozzi P (2001) Phonons and related crystal properties from density-functional perturbation theory. *Rev Mod Phys* 73: 515.
32. Lindemann FA (1910) *Phys Z* 11: 609.
33. Gilvarry JJ (1956) The Lindemann and Grüneisen Laws. *Phys Rev* 102: 308.
34. Errandonea D (2013) High-pressure melting curves of the transition metals Cu, Ni, Pd, and Pt. *Phys Rev B* 87: 054108.
35. Burakovsky L, Burakovsky N, Cawkwell MJ, Preston DL, Errandonea D, et al. (2016) Ab initio phase diagram of iridium. *Phys Rev B* 94: 094112.
36. Anzellini S, Monteseguro V, Bandiello E, Dewaele A, Burakovsky L, et al. (2019) In situ characterization of the high pressure – high temperature melting curve of platinum. *Sci Rep* 9: 13034.
37. Weck G, Recoules V, Queyroux JA, Datchi F, Bouchet J, et al. (2020) Determination of the melting curve of gold up to 110GPa. *Phys Rev B* 101: 014106.
38. Zhang Y, Tan Y, Geng HY, Salke NP, Gao Z, et al. (2020) Melting curve of vanadium up to 256GPa: Consistency between experiments and theory. *Phys Rev B* 102: 214104.
39. Anand K, Rajesh K, Sharma VS (2022) Melting curves of diatomic solids using the Lindemann law and a density-dependent Grüneisen parameter. *Comp Cond Matter* 30: e00647.
40. Zerr A, Boehler R (1994) Constraints on the melting temperature of the lower mantle from high-pressure experiments on MgO and magnesioüstite. *Nature (London)* 371: 506-508.
41. Boehler R, Ross M, Boercker DB (1997) Melting of LiF and NaCl to 1 Mbar: Systematics of ionic solids at extreme conditions. *Phys Rev Lett* 78(24): 4589.
42. Cazorla C, Errandonea D (2014) Superionicity and polymorphism in calcium fluoride at high pressure. *Phys Rev Lett* 113(23): 235902.
43. Vočadlo L, Price GD (1996) The melting of MgO-computer calculations via molecular dynamics. *Phys Chem Minerals* 23: 42-49.
44. Boehler R, Ross M, Boercker DB (1996) High-pressure melting curves of alkali halides. *Phys Rev B* 53(2): 556.
45. Belonoshko AB, Dubrovinsky LS (1996) Molecular dynamics of NaCl (B1 and B2) and MgO (B1) melting; two-phase simulation. *Am Mineral* 81(3-4): 303-316.
46. Alfe D (2005) Melting curve of MgO from first-principles simulations. *Phys Rev Lett* 94(23): 235701.
47. Anderson OL (1995) *Equations of state of solids for geophysics and ceramic science*. Oxford University Press, UK.
48. Shanker J, Kushwah SS, Kumar P (1997) Theory of thermal expansivity and bulk modulus for MgO and other minerals at high temperatures. *Physica B* 233(1): 78-83.
49. Shanker J, Sharma MP, Kushwah SS (1999) Analysis of melting of ionic solids based on the thermal equation of state. *J Phys Chem Solids* 60(5): 603-606.
50. Mao PL, Yu B, Liu Z, Wang F, Ju Y (2014) Mechanical properties and electronic structures of MgCu₂, Mg₂Ca and MgZn₂ laves phases by first principles calculations. *Trans Nonferrous Met Soc China* 24(9): 2920-2929.

-
51. Shanker J, Anand K, Sharma BS, Vijay A (2020) On the applicability of Lindemann's law for the melting of alkali metals. *Int J Thermophys* 41: 170.
52. Stacey FD, Davis PM (2004) High pressure equations of state with applications to the lower mantle and core. *Phys Earth Planet Int* 142(3-4): 137-184.
53. Stacey FD (2005) High pressure equations of state and planetary interiors. *Rep Prog Phys* 68: 341.
54. Shanker J, Sunil K, Sharma BS (2012) Formulation of the third-order Grüneisen parameter at extreme compression. *Physica B* 407(12): 2082-2083.
55. Shanker J, Sunil K, Sharma BS (2017) The Grüneisen parameter and its higher order derivatives for the earth lower mantle and core. *Phys Earth Planets Inter* 262: 41-47.